Carbohydrate Polymers 92 (2013) 469–478

Contents lists available at SciVerse ScienceDirect

Carbohydrate Polymers

journal homepage: www.elsevier.com/locate/carbpol

In situ observation of crystallinity disruption patterns during starch gelatinization

Canhui Cai[a,b], Cunxu Wei[a,b,*]

[a] Key Laboratories of Crop Genetics and Physiology of the Jiangsu Province and Plant Functional Genomics of the Ministry of Education, Yangzhou University, Yangzhou 225009, China
[b] College of Bioscience and Biotechnology, Yangzhou University, Yangzhou 225009, China

ARTICLE INFO

Article history:
Received 19 June 2012
Received in revised form 17 August 2012
Accepted 27 September 2012
Available online 4 October 2012

Keywords:
Starch granule
Gelatinization
Swelling
In situ observation
Polarizing microscope with hot stage

ABSTRACT

Twelve starches were isolated from the tuberous root of sweet potato, the rhizomes of lotus and yam, the tuber of potato, the corm of water chestnut, and the seeds of pea, bean, barley, wheat, lotus, water caltrop, and ginkgo. Their gelatinization processes were in situ viewed using a polarizing microscope in combination with a hot stage. Four patterns of crystallinity disruption during heating were proposed. The crystallinity disruption initially occurred on the proximal surface of the eccentric hilum, on the distal surface of the eccentric hilum, from the central hilum, or on the surface of the central hilum starch granule. The patterns of initial disruption on the distal surface of the eccentric hilum and on the surface of the central hilum starch were reported for the first time. The heterogeneous distribution of amylose in starch granule might partly explain the different patterns of crystallinity disruption and swelling during gelatinization.

1. Introduction

Starch is produced by plants where it is stored as discrete semicrystalline granules, and consists of two main components: mainly linear amylose and highly branched amylopectin (Gallant, Bouchet, & Baldwin, 1997). Previous researches from electron microscopy show that the alternating semicrystalline and amorphous growth rings and the central amorphous starch region represent three distinct inner structural features of starch granules (Gallant et al., 1997; Li, Vasanthan, Hoover, & Rossnagel, 2003). Recently, Parker, Kirby, and Morris (2008) view the internal structure of starch granules using atomic force microscopy. Their results suggest that the granules contain alternating rings with different levels of crystallinity and different amylose/amylopectin ratios. Starches isolated from different botanical sources display characteristic granule morphologies. Starch granules vary in shape, including spherical, oval, polygonal, disk (lenticular), elongated and kidney shapes, and in size from <1 μm to 100 μm in diameter (Jane, 2009). The hilum, which is the core of the granule and the starting point from which the granule grows, is usually less organized than the rest of the granule. Most commonly it is situated near the middle of the granule, but it can be eccentric, i.e. towards one end of the granule (Gott, Barton, Samuel, & Torrence, 2006). According to the position of the hilum, starch granules have two types of central hilum granule and eccentric hilum granule.

Starch granules are insoluble in cold water. When starch is heated in the presence of enough water, granules absorb water and swell. The absorption of water by amorphous regions within the granules destabilizes their crystalline structure, results in the loss of birefringence, which is one definition of gelatinization (Parker & Ring, 2001). Gelatinization is an important factor contributing to starch functionality and is widely exploited in the food industry (Ratnayake & Jackson, 2007). Starch gelatinization and associated properties can be determined by various methods, including optical microscopy, electron microscopy, differential scanning calorimetry, X-ray diffraction, nuclear magnetic resonance spectroscopy, Fourier transform infrared spectroscopy, viscosity measurement, enzymatic digestibility, light extinction, and solubility or sedimentation of swollen granule (Liu, Charlet, Yelle, & Arul, 2002; Ratnayake & Jackson, 2006). All these methods measure slightly different physicochemical properties and have unique and inherent advantages and disadvantages.

The gelatinization behavior of individual starch granule can be examined using polarizing microscope with a hot stage. With the procedure, the disruption of crystalline structure and the swelling of disrupted areas can be clearly seen. For example, the sizes and distributions of potato and rice starch granules are determined using this procedure during gelatinization (Liu et al., 2002; Yeh & Li, 1996). The effect of heating rate on the morphology and size of wheat starch granule is also investigated using this procedure (Patel & Seetharaman, 2006). The disruption of crystalline structure during pea and potato starch gelatinization begins from the

* Corresponding author at: College of Bioscience and Biotechnology, Yangzhou University, Yangzhou 225009, China. Tel.: +86 514 87997217.
E-mail addresses: cxwei@yzu.edu.cn, yzuwcx@yahoo.com.cn (C. Wei).

0144-8617/$ – see front matter © 2012 Elsevier Ltd. All rights reserved.
http://dx.doi.org/10.1016/j.carbpol.2012.09.073

hilum area, is propagated along the granule and accompanied by swelling of disrupted areas (Bogracheva, Meares, & Hedley, 2006; Bogracheva, Morris, Ring, & Hedley, 1998; Tahir, Ellis, Bogracheva, Meares-Taylor, & Butterworth, 2011).

In this paper, 12 starches were isolated from a wide variety of plant sources, consisting of tuberous root, tuber, corm, rhizome and seeds. Their morphologies, amylose contents and crystalline properties were investigated. The gelatinization processes of granules were in situ viewed using a polarizing microscope in combination with a hot stage. Four patterns of crystallinity initial disruption and swelling during heating were proposed. The amylose distributions in native starch granules were also investigated using a confocal laser scanning microscope (CLSM) to explain the different gelatinization processes of starch granules. This study would be very useful for the understanding of the gelatinization processes of different starches and for further utilization of these starches.

2. Materials and methods

2.1. Plant material

The tuberous root of sweet potato (*Ipomoea batatas* L.), the rhizomes of lotus (*Nelumbo nucifera* Gaertn.) and yam (*Dioscorea opposita* Thunb.), the tuber of potato (*Solanum tuberosum* L.), the corm of water chestnut (*Eleocharis dulcis* (Burm. F.) Trin. ex Hensch.), and the seeds of pea (*Pisum sativum* L.), bean (*Vicia faba* L.), barley (*Hordeum valgare* L.), wheat (*Triticum aestivum* L.), lotus (*N. nucifera* Gaertn.), water caltrop (*Trapa bispinosa* Roxb.), and ginkgo (*Ginkgo biloba* L.) were used to isolate native starch. Freshly harvested sweet potato tuberous root, lotus and yam rhizomes, potato tuber, water chestnut corm, water caltrop seed, and mature dry seeds of pea, bean, lotus and ginkgo were obtained from a local natural food market (Yangzhou City, China). Barley and wheat mature seeds were harvested in the experiment field of Yangzhou University, Yangzhou, China.

2.2. Isolation of native starches

Native starches were isolated following a method described by Man et al. (2012). Briefly, the seeds of pea, bean, barley, wheat and lotus were steeped overnight in double-distilled water at 4 °C. Sweet potato tuberous root, lotus and yam rhizomes, potato tuber and water chestnut corm were peeled and sliced into small pieces. The hard seed coats of ginkgo and water caltrop were removed with the help of a sharp and clean stainless steel knife and the edible portions were used to isolate starches. These above materials were homogenized with ice-cold water in a home blender. The homogenate was filtered with 100-, 200-, and 300-mesh sieves, successively. The starch suspension was centrifuged at 3000 × *g* for 10 min. The yellow gel-like layer on top of the packed white starch granule pellet was carefully scraped off and discarded. The process of centrifugation separation was repeated several times until no dirty material existed. The precipitated starch was further washed two times with anhydrous ethanol, dried at 40 °C for 2 days, ground into powders, and passed through a 100-mesh sieve. The starch samples were stored at −20 °C for analysis.

2.3. Morphology observation of starches

A starch suspension (1%) was prepared with 50% glycerol. A small drop of starch suspension was placed on the microscope slide and covered with a coverslip. The granule shape and Maltese cross were viewed under the Olympus BX53 polarizing light microscope equipped with a CCD camera.

2.4. Light microscope with hot stage

Starch suspensions were prepared by suspending about 10 mg starch in 1.0 ml of water by using a vortex mixer. The suspension was transferred onto a slide, covered with a coverslip, and sealed with nail polish to prevent moisture loss during heating. The sealed specimen was then mounted on a Kitazato hot stage apparatus and observed under a long focus M Plan Semi Apochromat objective (50× magnification) using the Olympus polarizing microscope equipped with cross polarizers and λ-plate during heating. The hot stage was heated from 25 to 50 °C at a heating rate of 5 °C/min and from 50 to 90 °C at a heating rate of 1 °C/min. The behavior of individual starch granule during heating was viewed under normal and polarizing light and photographed using an Olympus DP72 CCD camera.

2.5. Confocal laser scanning microscope

Starch granules were prepared for CLSM essentially as previously described (Blennow et al., 2003). Briefly, starch granules (about 2 mg) were stained in 3 μl of APTS solution (20 mM 8-amino-1,3,6-pyrenetrisulfonic acid (molecular probes, Sigma–Aldrich) dissolved in 15% acetic acid) and 3 μl of 1 M sodium cyanoborohydride. Samples were incubated at 30 °C for 15 h, washed five times in double-distilled water and suspended in 20 μl of 50% glycerol. 2 μl of the starch granule suspension was added to 8 μl of a highly viscous mixture containing 2% agar and 85% glycerol in water. The sample thoroughly mixed using a plastic pipette tip. The sample was immediately mounted on a glass plate for microscopy. Images were recorded on a CLSM (LSM 710, Carl Zeiss MicroImaging GmbH, Jena, Germany) using a 488 nm laser line for excitation and light was detected in the interval from 500 to 535 nm. Image analysis was performed using the Carl Zeiss ZEN 2010 software and granules were viewed using the channels from red to white.

2.6. Amylose content determination of starches

Amylose content was determined following a modified method (Man et al., 2012) according to the iodine adsorption method of Konik-Rose et al. (2007). The experiments were performed thrice.

2.7. Crystalline property of starches

Crystalline property of starches was analyzed on an X-ray powder diffraction (XRD) (D8, Bruker, Germany) following the method described by Wei et al. (2010).

3. Results and discussion

3.1. Morphology of starches

Photomicrographs of starch granules taken from polarizing light microscope under normal light and polarizing light are presented in Fig. 1. Potato starch had large and small granules, they showed the oval and spherical shapes, respectively (Fig. 1A). The hilum positions of potato oval and spherical starches were at one end of granules (Fig. 1a). Lotus rhizome starch showed significantly heterogeneous shapes, including elongated, oval, spherical and irregular shapes. The elongated and oval granules were larger than the spherical and irregular ones (Fig. 1B). The hilum positions were at one end of granules (Fig. 1b). Yam starch was slightly oval with the hilum at one end of granules (Fig. 1C and c). Pea and bean starches were oval with the hilum in the center of granules (Fig. 1D, d, E and e). Barley and wheat starches had bimodal size distributions, the large granules had disk shapes, whereas the small granules had spherical shapes. Their hilum positions were all in the

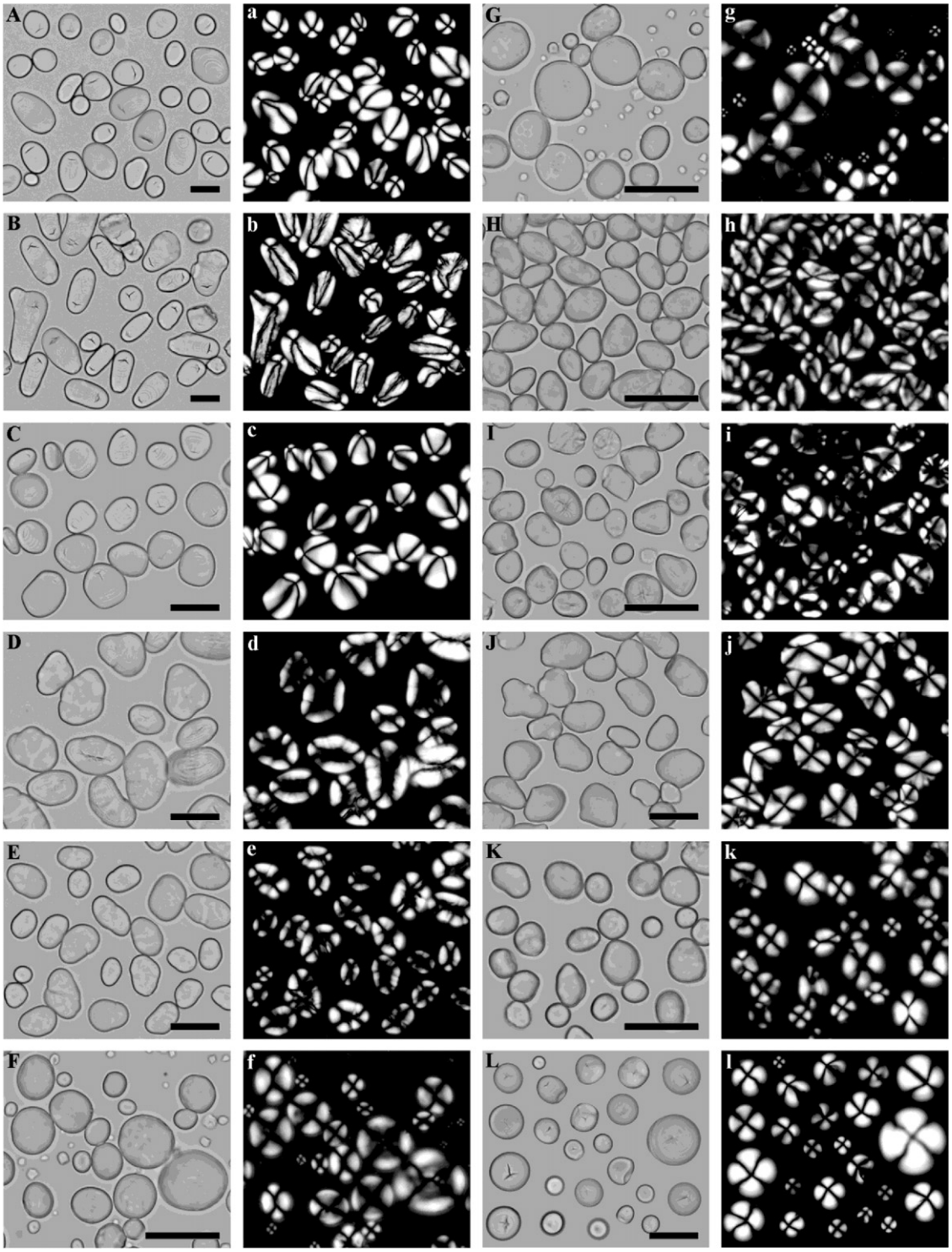

Fig. 1. Morphology of starch granule. (A–L) Normal light microscope graphs; (a–l) polarizing light microscope graphs; (A, a) potato; (B, b) lotus rhizome; (C, c) yam; (D, d) pea; (E, e) bean; (F, f) barley; (G, g) wheat; (H, h) lotus seed; (I, i) water chestnut; (J, j) water caltrop; (K, k) ginkgo; (L, l) sweet potato. Scale bar = 20 μm.

center of granules (Fig. 1F, f, G, and g). Lotus seed, water chestnut and water caltrop starches were mostly oval with the central hila (Fig. 1H–J and h–j). Ginkgo starch had large oval and small spherical granules, their hila were in the center of granules (Fig. 1K and k). Most of sweet potato starch was spherical granules with central hila and significantly different sizes, some of sweet potato starch was oval granules with hila at one end of granules (Fig. 1L and l). Among these starches, potato, lotus rhizome, barley and wheat starches were the most heterogeneous in shape and size. The differences in granule shape and hilum position might be attributed to the biological origin, biochemistry of the amyloplast and physiology of the plant (Sandhu, Singh, & Kaur, 2004).

3.2. Different patterns of starch granule disruption on heating

The behaviors of starch granules during gelatinization were viewed by observing granular birefringence using polarizing microscope with a λ plate in combination with a hot stage (Figs. 2–6).

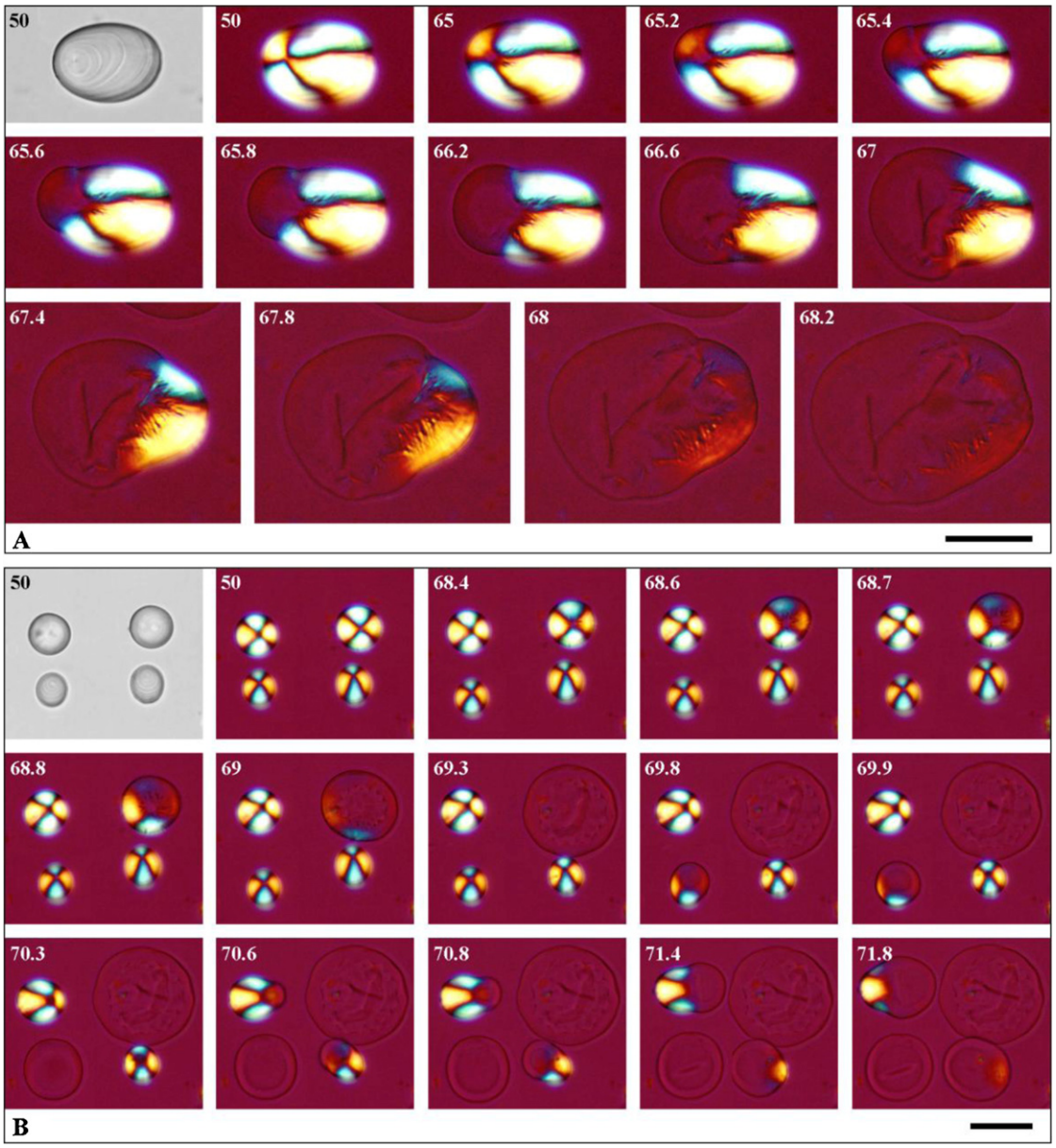

Fig. 2. Micrographs of potato starch granules viewed under normal and polarizing light in conjunction with a λ plate during heating. (A) Large starch granule; (B) small starch granule. The number in the top left corner of each micrograph represents the corresponding heating temperature (°C). Scale bar = 20 μm. (For interpretation of the references to color in text, the reader is referred to the web version of this article.)

With this procedure, the effect of heating on granular structure and swelling could be seen in the micrographs. The blue and yellow areas represented regions of the granules containing crystallites. These colors disappeared as the crystallites were disrupted during heating. The swelling of disrupted areas could be clearly seen in the micrographs (Tahir et al., 2011). Generally, starch granules showed their intact shapes before gelatinization as observed under normal light, were birefringent and showed the characteristic "Maltese cross" pattern under polarizing light. Birefringence patterns indicated a radial alignment of crystallites within starch granules, and the loss of birefringence on heating, indicative of disordering processes, suggested the loss of radially aligned crystallites (Pérez, Baldwin, & Gallant, 2009). During gelatinization, swelling was accompanied by the rupture of granule (loss of birefringence). When the loss of birefringence began, most of the granules were partially swollen. The regular orientation of D-glucosyl units in amorphous and crystalline regions disappeared, the swelling became irreversible and the characteristic "Maltese cross" pattern disappeared under polarizing light with increase in heating temperature. Finally, the birefringence of starch granules disappeared completely, the disrupted parts of the granules became the same color as the background, and gelatinization process was over. During starch gelatinization, the disruption of crystallinity in a particular area of the granule increased the swelling capacity of this area. The swollen disrupted parts of the granule had much higher water content than the amorphous part of undisturbed areas. It was evident that the swelling of disturbed areas accelerated the process of disruption of neighboring crystallinities, and that this process was rapidly propagated along the granule (Bogracheva et al., 1998). In this paper, the gelatinization processes of more than 100 starch granules with different sizes and shapes from each sample were in situ observed. Apart from sweet potato starch, granules from the same sample showed the same disruption pattern though they had different sizes and shapes. The gelatinization process was more evident for large granule than small granule. Therefore, only a typical micrograph of

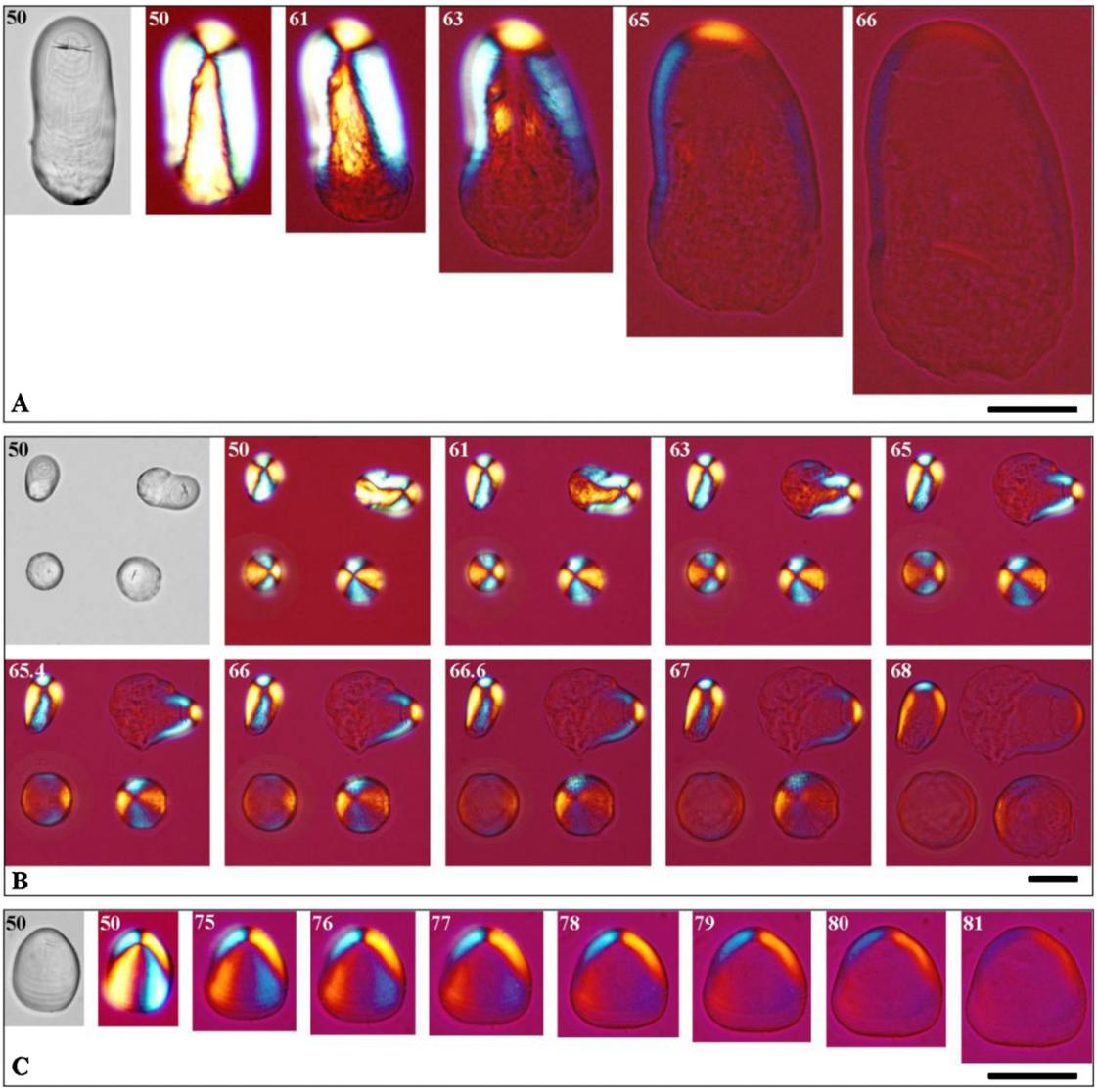

Fig. 3. Micrographs of lotus (A and B) and yam (C) rhizome starch granules viewed under normal and polarizing light in conjunction with a λ plate during heating. (A) Large starch granule; (B) small starch granule. The number in the top left corner of each micrograph represents the corresponding heating temperature (°C). Scale bar = 20 μm. (For interpretation of the references to color in text, the reader is referred to the web version of this article.)

large granule from most samples was shown to stand for the disruption pattern of each granule type. According to the initial position of birefringence disappearance and granule swelling during heating, four patterns of crystallinity initial disruption and swelling were proposed during gelatinization.

Fig. 2 shows the gelatinization processes of potato large and small starch granules. Before gelatinization, starch granules kept intact morphology. Under normal light, potato large starch granule had a clear eccentric hilum and many growth rings. Under polarizing light, potato starch granules had the "Maltese cross" with bright birefringence. When gelatinization began, the disruption of crystalline structure firstly occurred on the proximal surface of the eccentric hilum. The disruption of crystalline structure was almost simultaneous with the granule swelling. It was clear that the disruption of crystalline structure, accompanied by swelling, was propagated along the granules from the proximal surface to the distal surface of the eccentric hilum. Potato large and small starch granules showed the same disruption pattern though they had different shapes and sizes. The gelatinization process of potato starch was similar to that observation of Bogracheva et al. (2006). Therefore, the first pattern of starch gelatinization indicated that crystallinity disruption initially occurred on the proximal surface of the eccentric hilum.

Fig. 3 shows the micrographs of lotus and yam rhizome starch granules during heating. Before gelatinization, lotus and yam rhizome starches also presented the eccentric hila and bright "Maltese crosses", which was similar to that of potato starch granule. However, the gelatinization processes of lotus and yam rhizome starches were wholly contrary to that of potato starch granule. When gelatinization began, the disruption of crystalline structure firstly occurred on the distal surface of the eccentric hilum. The disruption of crystalline structure and granule swelling were propagated along the granules from the distal surface to the proximal surface of the eccentric hilum. Though lotus rhizome starch granules had significantly different shapes and sizes, their hilum positions were all at one end of granules, and their disruption patterns were all the same. This pattern of gelatinization processes for lotus and yam rhizome starches was never reported, which was the second pattern of starch gelatinization.

Fig. 4 shows the micrographs of pea, bean, barley, wheat and lotus seed starches and water chestnut corm starch during heating. Though their morphologies were significantly different, but they all

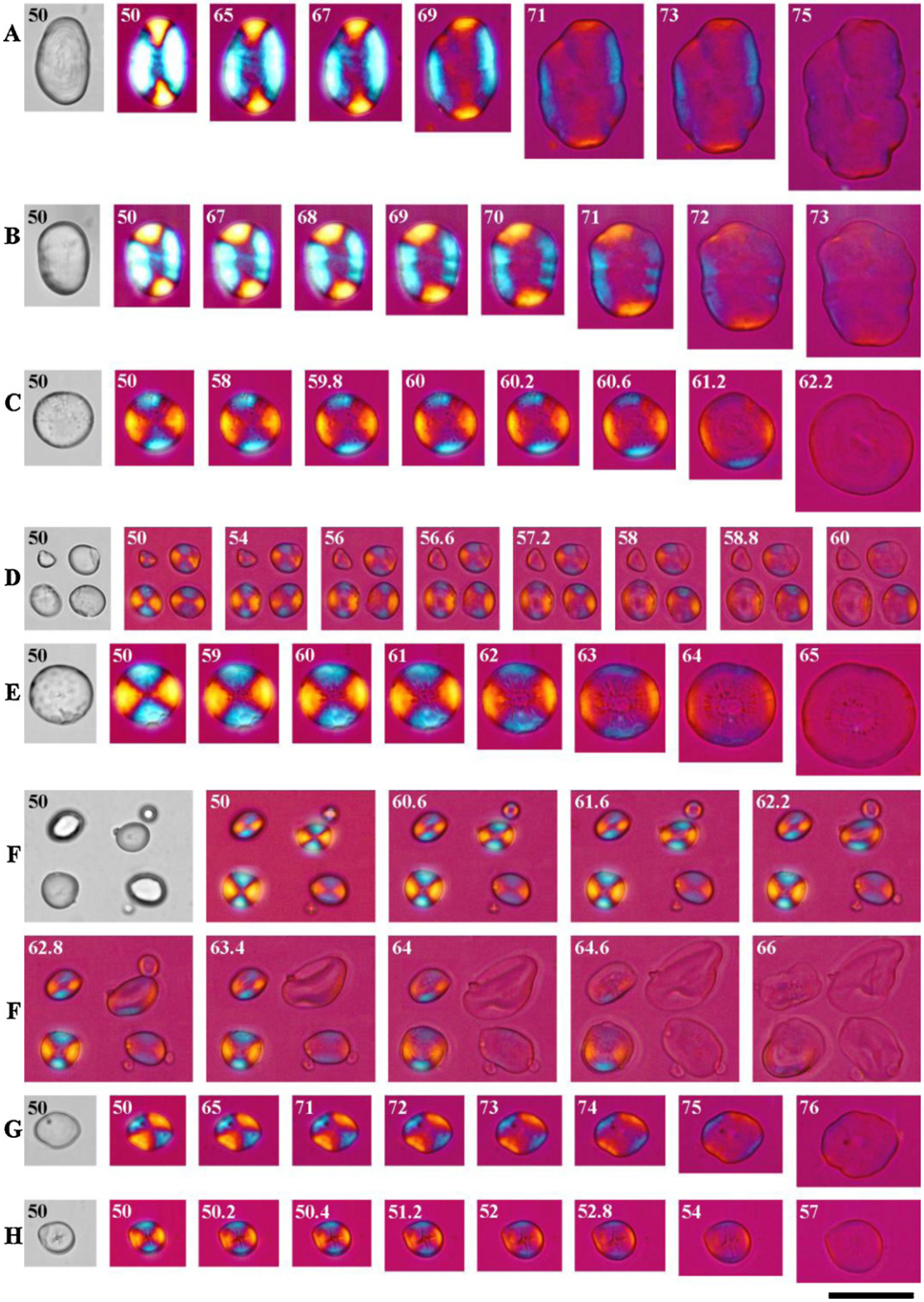

Fig. 4. Micrographs of pea (A), bean (B), barley (C and D), wheat (E and F), lotus seed (G) and water chestnut (H) starch granules viewed under normal and polarizing light in conjunction with a λ plate during heating. (C and E) Large starch granule; (D and F) small starch granule. The number in the top left corner of each micrograph represents the corresponding heating temperature (°C). Scale bar = 20 μm. (For interpretation of the references to color in text, the reader is referred to the web version of this article.)

showed the central hila. Their gelatinization processes were also similar. The crystallinity disruption during gelatinization began from the hilum area and was propagated along the central part of the granule, accompanied by a small amount of swelling. As the temperature increased, the crystallinity continued to disrupt and swell from the inner to the outer of starch granule. During this stage, the crystalline structure of the outer part of the granule remained undisrupted. The last stage of the gelatinization process was the crystallinity disruption of the granule surface. The completely disrupted granule rapidly became highly swollen along the surface.

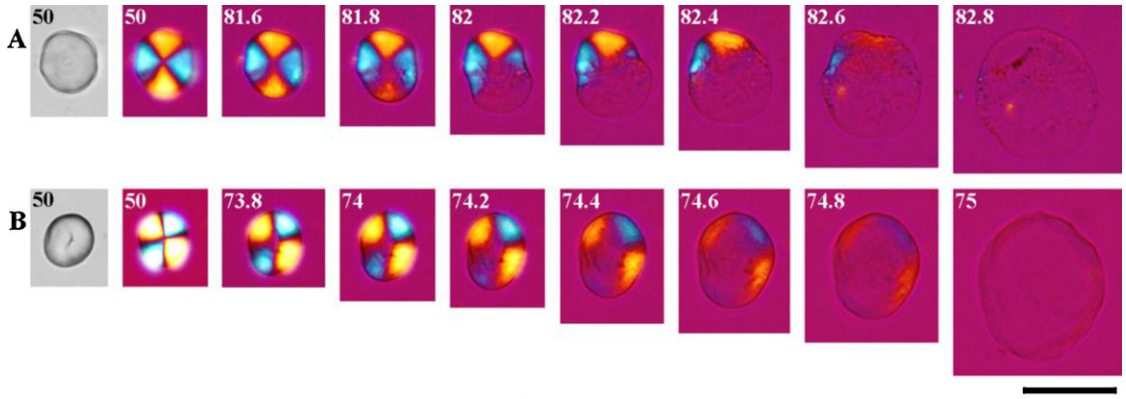

Fig. 5. Micrographs of water caltrop (A) and ginkgo (B) starch granules viewed under normal and polarizing light in conjunction with a λ plate during heating. The number in the top left corner of each micrograph represents the corresponding heating temperature (°C). Scale bar = 20 μm. (For interpretation of the references to color in text, the reader is referred to the web version of this article.)

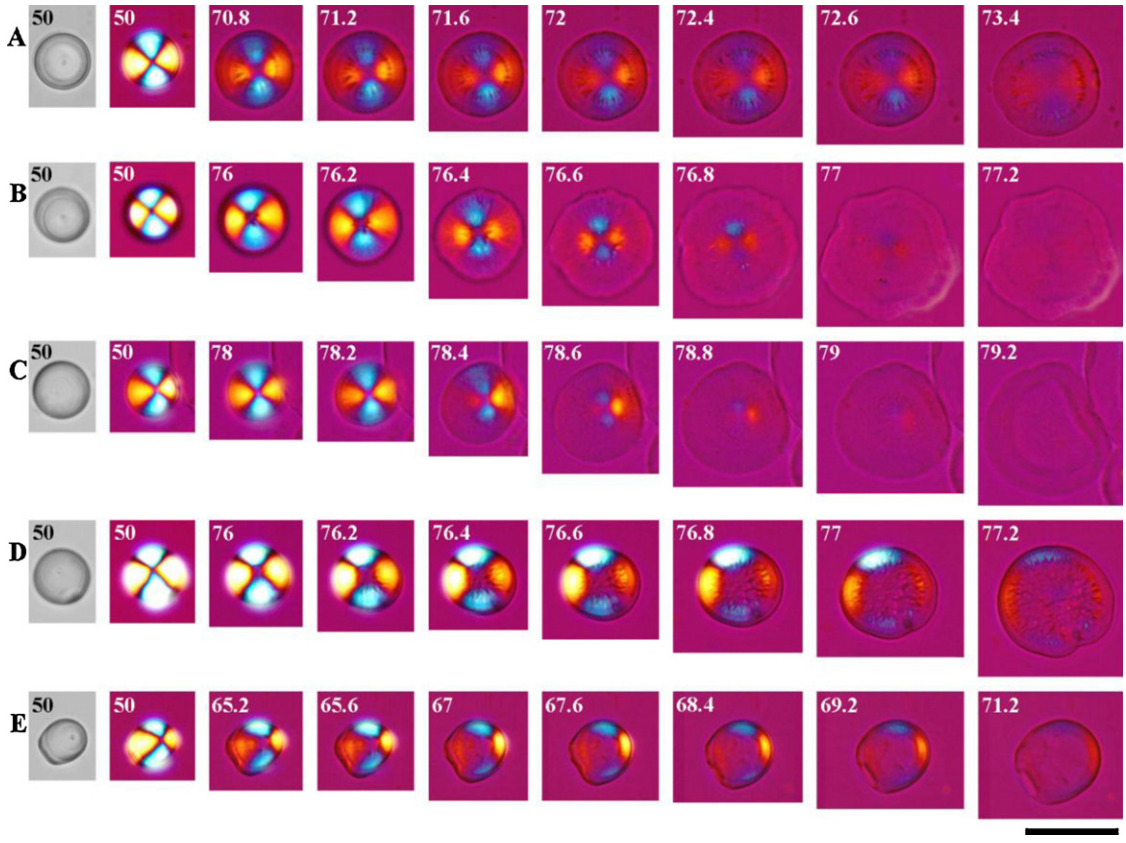

Fig. 6. Micrographs of sweet potato starch granules viewed under normal and polarizing light in conjunction with a λ plate during heating. The number in the top left corner of each micrograph represents the corresponding heating temperature (°C). Scale bar = 20 μm. (For interpretation of the references to color in text, the reader is referred to the web version of this article.)

Barley and wheat large and small starch granules with significantly different shapes and sizes showed the same disruption pattern. This pattern of crystallinity disruption and swelling was in agreement with previous reports of pea starch (Bogracheva et al., 1998; Tahir et al., 2011), which was the third pattern of starch gelatinization.

Fig. 5 shows the micrographs of water caltrop and ginkgo starch granules during heating. Water caltrop and ginkgo starches also showed the central hila, the crystallinity disruption during gelatinization began from the hilum area, which was similar to that of Fig. 4, but the subsequent process was significantly different from that of Fig. 4. With heating temperature increasing, the crystallinity disruption and swelling was propagated from the central hilum to one side surface of the granule, and then from the disrupted side surface to the undisrupted side surface of the granule. Though starch granules in Fig. 5 shows some differences from that of Fig. 4 in crystallinity disruption and swelling, their initial disruption and swelling also occurred from the central hilum area, which belonged to the third pattern of starch gelatinization.

Fig. 6 shows the gelatinization processes of sweet potato starch granules. Sweet potato starch granules had many gelatinization patterns. Before gelatinization, some sweet potato starch granules showed spherical shape with the central hila, other starch granules showed oval shape with eccentric hila. The gelatinization processes of some spherical starch granules with central hilum indicated

that the crystallinity disruption and swelling initially occurred on the outer surface of the granule, then the subsequent disruption and swelling was propagated from the outer to the inner of the granule, and the crystallinity around the central hilum was finally disrupted and swelled (Fig. 6A–C). This pattern of gelatinization process was reported for the first time, we defined it as the fourth pattern of starch gelatinization. There were some spherical sweet potato starch granules with central hila, they showed that the crystallinity disruption and swelling initially occurred from the hilum area and was propagated from the inner to the outer of the granule (Fig. 6D). This pattern of gelatinization process was similar to that of pea starch, and belonged to the third pattern of starch gelatinization. The oval sweet potato starch granule with the eccentric hilum showed that crystallinity disruption and swelling firstly occurred on the distal surface of the eccentric hilum and was propagated along the granules from the distal surface to the proximal surface of the eccentric hilum (Fig. 6E). This pattern of gelatinization process was similar to that of lotus and yam rhizome starches, and belonged to the second pattern of starch gelatinization.

3.3. Amylose content and distribution in starch granules

Starch consisted of two main components: amylose and amylopectin, the amylose content plays an important role in starch internal quality and its property (Gallant et al., 1997). In this paper, the amylose contents of starches are listed in Table 1. These starches were all normal starches rather than waxy or high-amylose starches. Among them, lotus rhizome and barley starches showed the lowest amylose content (23.9%), and pea starch showed the highest amylose content (44.4%).

During starch gelatinization, amylopectin was considered to contribute to water absorption and swelling and pasting of starch granules, whereas amylose tended to retard these processes (Tester & Morrison, 1990). The linear amylose diffused out of the swollen granules and made up the continuous phase outside the granules as a restraint to swelling. So, an inverse correlation was found between amylose content and swelling power (Hermansson & Svegmark, 1996). Tester and Morrison (1990) reported that starch granular swelling was primarily a property of amylopectin and that amylose appeared to act as a diluent. The method for visualizing the distribution of amylose and amylopectin in starch granules was developed using the fluorophore ATPS, which specifically reacted with the reducing end of starch molecules leading to a 1:1 stoichiometric ratio of starch molecule labeling. Because of its smaller size, amylose contained a much higher molar ratio of reducing ends per glucose residue than amylopectin. This resulted in a higher by-weight labeling of amylose and enabled the distinction of amylose and amylopectin by CLSM (Blennow et al., 2003; Glaring, Koch, & Blennow, 2006). In order to explain the different patterns of crystallinity disruption and swelling, equimolar labeling of starch molecules with APTS was used to construct a detailed map of the distribution of amylose and amylopectin within the granule by CLSM analysis in this paper.

The distributions of amylose in native starch granules were shown in Fig. 7. Many starch granules with different sizes and shapes from each sample were viewed for the amylose distribution. Apart from sweet potato starch, granules from the same sample showed the similar distribution of amylose though they had different sizes and shapes. Therefore, only a typical micrograph of granule was shown to stand for the amylose distribution of each granule type (apart from sweet potato starch). Apart from sweet potato starch, the CLSM image of each granule type corresponded to its polarizing microscope image. The color from black to red, orange, yellow and white represented the fluorescence intensity (i.e. amylose content) from low to high according to the analysis software. CLSM optical section of potato starch granule showed clear growth rings around an eccentric hilum. An intense fluorescence in the amorphous growth rings between the hilum and its distal surface indicated that a high concentration of amylose in this region (Fig. 7A). CLSM optical sections of yam and lotus rhizome starches also showed clear growth rings around an eccentric hilum. However, the high concentration of amylose was distributed in the amorphous growth rings between the hilum and its proximal surface, which was wholly contrary to that of potato starch (Fig. 7B and C). Compared the distribution of amylose with the initial disruption and swelling of crystalline structure in potato tuber and lotus and yam rhizome starches, we could conclude that the amylose in the amorphous growth rings might restrain crystallinity disruption and swelling. Furthermore, lipid-complexed amylose chains restricted both granular swelling and amylose leaching (Tester & Morrison, 1992). Therefore, the crystallinity disruption and swelling began from the surface of low amylose concentration in eccentric hilum starches.

CLSM optical sections of pea and bean starches showed clear growth rings around a central hilum that was irregular. The amylose was mainly distributed in the hilum area and the amorphous growth rings (Fig. 7D and E). The amylose distribution in the amorphous growth rings was even and symmetrical in pea and bean starches, which was different from that in potato, lotus and yam rhizome starches with regional distribution. Though the

Table 1
Amylose content, crystalline type, morphology and gelatinization pattern of starch.

Starch	Amylose content (%)	Crystalline type	Morphology		Gelatinization pattern[a]
			Shape	Hilum position	
Potato	34.7 ± 1.7	B	Oval, spherical	Terminal	P1
Lotus rhizome	23.9 ± 0.4	C	Elongated, oval, spherical	Terminal	P2
Yam	34.7 ± 0.9	C	Oval	Terminal	P2
Pea	44.4 ± 1.3	C	Oval	Central	P3
Bean	40.0 ± 0.5	C_A [b]	Oval	Central	P3
Water chestnut	27.9 ± 1.2	C_A [b]	Oval	Central	P3
Barley	23.9 ± 1.1	A	Disk, spherical	Central	P3
Wheat	28.9 ± 1.0	A	Disk, spherical	Central	P3
Lotus seed	39.2 ± 1.5	A	Oval	Central	P3
Water caltrop	25.7 ± 0.5	A	Oval	Central	P3
Ginkgo	29.9 ± 0.9	A	Oval, spherical	Central	P3
Sweet potato	25.6 ± 0.9	A	Spherical	Central	P3
			Oval	Terminal	P2
			Spherical	Central	P4

[a] P represent the gelatinization pattern that the crystallinity disruption initially occurs on the proximal surface of the eccentric hilum (P1), on the distal surface of the eccentric hilum (P2), from the central hilum (P3), and on the surface of the central hilum granule (P4).
[b] C_A-type starch is the C-type starch closer to A-type.

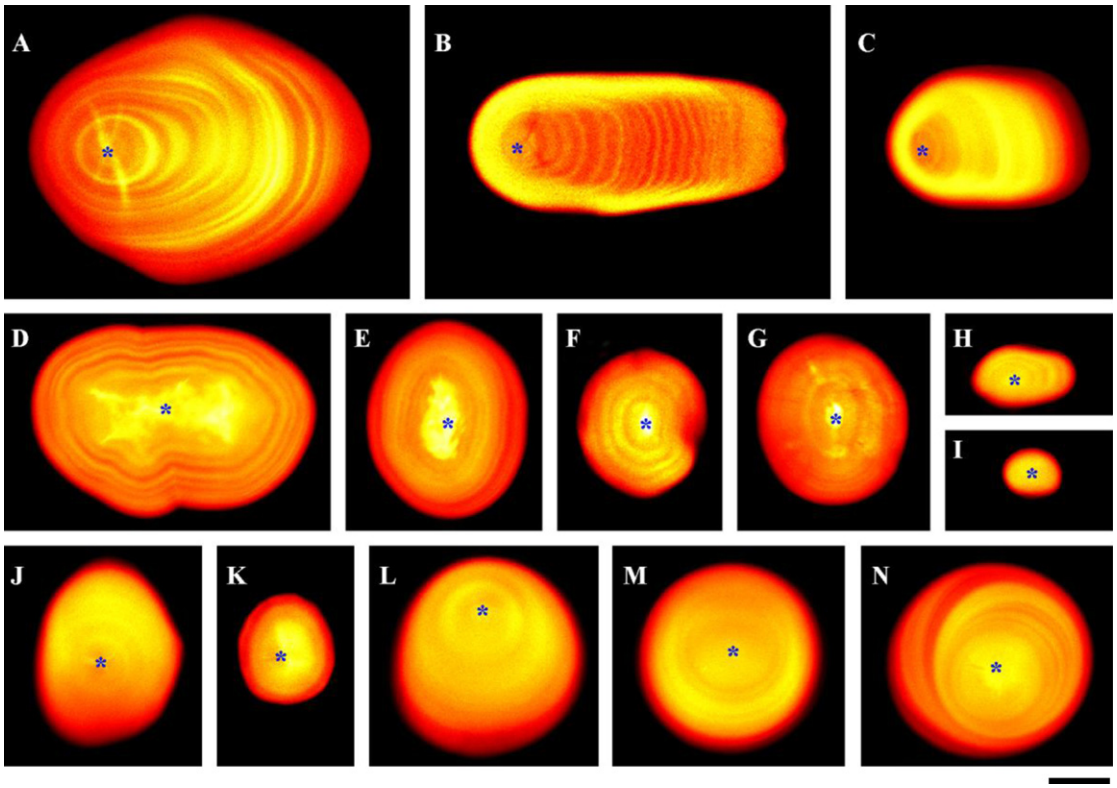

Fig. 7. Representative CLSM optical slices of APTS-stained starch granules from potato (A), lotus rhizome (B), yam (C), pea (D), bean (E), barley (F), wheat (G), lotus seed (H), water chestnut (I), water caltrop (J), ginkgo (K), and sweet potato (L–N). The blue asterisk indicates the hilum of starch granule. Scale bar = 10 μm. (For interpretation of the references to color in this figure legend, the reader is referred to the web version of this article.)

barley and wheat endosperm had large (A-type) and small (B-type) starch granules, our attention was focused mainly on large granules, because they represented the majority of the granule weight population of whole starch. In addition, it was easy to focus the large starch granules with high resolution using CLSM. CLSM optical sections of barley and wheat large starch granules showed clearly visible concentric growth rings around the central hilum, the amylose was mainly distributed in the central hilum and concentric growth rings, which was basically similar to that of pea and bean (Fig. 7F and G). CLSM optical sections of lotus seed and water chestnut corm starches revealed that the amylose distribution was similar to that of barley and wheat starches, though their sizes were significantly small (Fig. 7H and I). The amylose was mainly distributed around the central hilum and in amorphous growth rings in pea, bean, barley, wheat, and lotus seed starches and water chestnut corm starch (Fig. 7D–I). The crystallinity disruption and swelling of these starch granules began from the central hilum (Fig. 4). We thought that the structure and property of the amylose in hilum might be different from that of in amorphous growth rings. The amylose from hilum was released before crystallinity disruption, which resulted in a void in the hilum area and enabled crystallinity around the hilum area disrupt and swell.

CLSM optical sections of water caltrop and ginkgo seed starches showed the central hilum, the amylose was mainly distributed in amorphous growth rings (Fig. 7J and K). Though the crystallinity disruption and swelling initially occurred in the hilum, the local distribution of amylose resulted in crystallinity disruption and swelling in one direction. CLSM optical sections of sweet potato starch granules showed some different internal structures (Fig. 7L–N). For eccentric hilum sweet potato starch granules, amylose was mainly distributed in amorphous growth rings between hilum and its proximal surface (Fig. 7L), which was similar to that of yam starch. This distribution of amylose resulted in the pattern of crystallinity disruption and swelling (Fig. 6E) which was similar to that of lotus and yam rhizome starches (Fig. 3). For some central hilum starch granules, the amylose distribution was similar to that of water caltrop (Fig. 7M). Its disruption pattern (Fig. 6D) was also similar to that of water caltrop (Fig. 5A). For other central hilum starch granules, the amylose distribution was mainly in the hilum and in amorphous growth rings (Fig. 7N), which was similar to that of bean, barley and wheat starches, but the disruption and swelling pattern (Fig. 6A–C) was wholly contrary to that of bean, barley and wheat starches. The reason was worth further investigating.

3.4. Crystalline property of starches

Starch has A-, B- and C-type crystallinities according to XRD pattern. A-type crystal starches have strong diffraction peaks at about 15° and 23° 2θ, and an unresolved doublet at around 17° and 18° 2θ. B-type crystal starches give the strongest diffraction peak at around 17° 2θ, a few small peaks at around 15°, 20°, 22°, and 24° 2θ, and a characteristic peak at about 5.6° 2θ. C-type crystal starch is a mixture of both A- and B-type crystallinities, and can be further classified to C_A-type (closer to A-type), C-type and C_B-type (closer to B-type) according to the proportion of A-type and B-type polymorphs. The typical C-type crystal starches show strong diffraction peaks at about 17° and 23° 2θ, and a few small peaks at around 5.6° and 15° 2θ. C_A-type crystal starches show a shoulder peak at about 18° 2θ and strong peaks at about 15° and 23° 2θ, which are indicative of the A-type pattern. C_B-type crystal starches show two shoulder peaks at about 22° and 24° 2θ and a weak peak at about 15° 2θ, which are indicative of the B-type pattern (Cheetham & Tao, 1998). In this paper, the XRD patterns (data not shown) showed that barley, wheat, lotus seed, water caltrop, ginkgo and sweet potato starches were A-type crystallinities, potato starch was B-type crystallinity, lotus and yam rhizome starches and pea seed starch

were C-type crystallinites, and bean and water chestnut starches were C_A-type crystallinities (Table 1).

3.5. Amylose content, crystalline type, morphology and gelatinization pattern of starches

Starches had many disruption patterns during heating. Table 1 summarizes the amylose content, crystalline type, morphology and gelatinization pattern of starches. Amylose content had no effect on the disruption pattern. Starch granules were heterogeneous in shapes and sizes. The sizes of elongated, oval and disk granules were usual larger than that of spherical and irregular granules. Apart from sweet potato starch, granules from the same botanical source always showed the same disruption pattern though they had different shapes and sizes. The hilum position had a significant effect on the disruption pattern. The disruption initially occurred on the proximal or distal surface of the eccentric hilum. For the central hilum starches, the disruption occurred from the central hilum apart from sweet potato starch. The heterogeneous distribution of amylose in the eccentric starch granules might determine the disruption pattern. C-type starch was a mixture of A- and B-type allomorphs. For the C-type pea starch, the B-type polymorph was in the center of the granule and surrounded by the A-type polymorph. The arrangement of A- and B-type polymorphs played an important role in the swelling of the granules (Bogracheva et al., 1998). In this paper, C-type bean and water chestnut starches with central hila showed the similar disruption pattern with that of pea starch. However, the C-type lotus and yam rhizome starches with eccentric hila showed different disruption pattern from that of pea starch, which might result from the heterogeneous distribution of amylose in granule and the eccentric hila. It was not at present clear whether there were some effects of the allomorph distribution on crystallinity disruption pattern in C-type lotus and yam rhizome starches. The main reason was that lotus and yam rhizome starches were eccentric hilum granules which was different from the central hilum pea starch.

4. Conclusion

Morphology, amylose content and crystalline property of starches were investigated. The gelatinization processes of different starches were in situ viewed using a polarizing microscope in combination with a hot stage. There were four disruption patterns of crystalline structure during starch heating. For eccentric hilum starches, the crystallinity disruption and swelling initially occurred either on the proximal surface or on the distal surface of hilum. For central hilum starches, the crystallinity disruption and swelling began from the central hilum or on the whole surface of starch granule. Equimolar labeling of native starch molecules with APTS was used to construct a detailed map of the distribution of amylose and amylopectin within the granule by CLSM analysis. The heterogeneous distribution of amylose in starch granule might partly explain the different crystallinity disruption and swelling patterns of gelatinization starches.

Acknowledgments

The authors would like to thank the editor and two anonymous reviewers for valuable comments and suggestions to improve the quality of the manuscript. The authors are grateful to Prof. Qiaoquan Liu and Zhiyun Gong (Agricultural College, Yangzhou University, China) for providing instrument access and assistance with CLSM. This study was financially supported by grants from the National Natural Science Foundation of China (31071342, 31270221) and the Priority Academic Program Development from Jiangsu Government, China.

References

Blennow, A., Hansen, M., Schulz, A., Jørgensen, K., Donald, A. M., & Sanderson, J. (2003). The molecular deposition of transgenically modified starch in the starch granule as imaged by functional microscopy. *Journal of Structural Biology*, *143*, 229–241.

Bogracheva, T. Y., Meares, C., & Hedley, C. L. (2006). The effect of heating on the thermodynamic characteristics of potato starch. *Carbohydrate Polymers*, *63*, 323–330.

Bogracheva, T. Y., Morris, V. J., Ring, S. G., & Hedley, C. L. (1998). The granular structure of C-type pea starch and its role in gelatinization. *Biopolymers*, *45*, 323–332.

Cheetham, N. W. H., & Tao, L. (1998). Variation in crystalline type with amylose content in maize starch granules: An X-ray powder diffraction study. *Carbohydrate Polymers*, *36*, 277–284.

Gallant, D. J., Bouchet, B., & Baldwin, P. M. (1997). Microscopy of starch: Evidence of a new level of granule organization. *Carbohydrate Polymers*, *32*, 177–191.

Glaring, M. A., Koch, C. B., & Blennow, A. (2006). Genotype-specific spatial distribution of starch molecules in the starch granules: A combined CLSM and SEM approach. *Biomacromolecules*, *7*, 2310–2320.

Gott, B., Barton, H., Samuel, D., & Torrence, R. (2006). Biology of starch. In R. Torrence, & H. Barton (Eds.), *Ancient starch research* (pp. 35–45). Walnut Creek, CA: Left Coast Press.

Hermansson, A. M., & Svegmark, K. (1996). Developments in the understanding of starch functionality. *Trends in Food Science and Technology*, *7*, 345–353.

Jane, J. L. (2009). Structural features of starch granules II. In J. BeMiller, & R. Whistler (Eds.), *Starch: Chemistry and technology* (3rd ed., pp. 193–236). Amsterdam: Academic Press.

Konik-Rose, C., Thistleton, J., Chanvrier, H., Tan, I., Halley, P., Gidley, M., et al. (2007). Effects of starch synthase IIa gene dosage on grain protein and starch in endosperm of wheat. *Theoretical and Applied Genetics*, *115*, 1053–1065.

Li, J. H., Vasanthan, T., Hoover, R., & Rossnagel, B. G. (2003). Starch from hull-less barley: Ultrastructure and distribution of granule-bound proteins. *Cereal Chemistry*, *80*, 524–532.

Liu, Q., Charlet, G., Yelle, S., & Arul, J. (2002). Phase transition in potato starch-water system I starch gelatinization at high moisture level. *Food Research International*, *35*, 397–407.

Man, J. M., Cai, J. W., Cai, C. H., Xu, B., Huai, H. Y., & Wei, C. X. (2012). Comparison of physicochemical properties of starches from seed and rhizome of lotus. *Carbohydrate Polymers*, *88*, 676–683.

Parker, M. L., Kirby, A. R., & Morris, V. J. (2008). In situ imaging of pea starch in seeds. *Food Biophysics*, *3*, 33–76.

Parker, R., & Ring, S. G. (2001). Aspects of the physical chemistry of starch. *Journal of Cereal Science*, *34*, 1–17.

Patel, B. K., & Seetharaman, K. (2006). Effect of heating rate on starch granule morphology and size. *Carbohydrate Polymers*, *65*, 381–385.

Pérez, S., Baldwin, P. M., & Gallant, D. J. (2009). Structural features of starch granules I. In J. BeMiller, & R. Whistler (Eds.), *Starch: Chemistry and technology* (3rd ed., pp. 149–192). Amsterdam: Academic Press.

Ratnayake, W. S., & Jackson, D. S. (2006). Gelatinization and solubility of corn starch during heating in excess water: New insights. *Journal of Agricultural and Food Chemistry*, *54*, 3712–3716.

Ratnayake, W. S., & Jackson, D. S. (2007). A new insight into the gelatinization process of native starches. *Carbohydrate Polymers*, *67*, 511–529.

Sandhu, K. S., Singh, N., & Kaur, M. (2004). Characteristics of the different corn types and their grain fractions: Physicochemical, thermal, morphological and rheological properties of starches. *Journal of Food Engineering*, *64*, 119–127.

Tahir, R., Ellis, P. R., Bogracheva, T. Y., Meares-Taylor, C., & Butterworth, P. J. (2011). Study of the structure and properties of native and hydrothermally processed wild-type lam and *r* variant pea starches that affect amylolysis of these starches. *Biomacromolecules*, *12*, 123–133.

Tester, R. F., & Morrison, W. R. (1990). Swelling and gelatinization of cereal starches. I. Effects of amylopectin amylose and lipids. *Cereal Chemistry*, *67*, 551–557.

Tester, R. F., & Morrison, W. R. (1992). Swelling and gelatinization of cereal starches. III. Some properties of waxy and normal nonwaxy barley starches. *Cereal Chemistry*, *69*, 654–658.

Wei, C. X., Qin, F. L., Zhou, W. D., Chen, Y. F., Xu, B., Wang, Y. P., et al. (2010). Formation of semi-compound C-type starch granule in high-amylose rice developed by antisense RNA inhibition of starch-branching enzyme. *Journal of Agricultural and Food chemistry*, *58*, 11097–11104.

Yeh, A. I., & Li, J. Y. (1996). A continuous measurement of swelling of rice starch during heating. *Journal of Cereal Science*, *23*, 277–283.